Università degli Studi di Padova

Padua Research Archive - Institutional Repository

Re-emergence of modular brain networks in stroke recovery

(Article begins on next page)

Re-emergence of modular brain networks in stroke recovery

Joshua S. Siegel[a,*], **Benjamin A. Seitzman**[a], **Lenny E. Ramsey**[a], **Mario Ortega**[a], **Evan M. Gordon**[f], **Nico U.F. Dosenbach**[a], **Steven E. Petersen**[a,b,c,d], **Gordon L. Shulman**[a], and **Maurizio Corbetta**[a,b,c,e,g]

[a]Departments of Neurology, Washington University School of Medicine, St. Louis, MO, USA

[b]Mallinckrodt Institute of Radiology, Washington University School of Medicine, St. Louis, MO, USA

[c]Department of Psychology, Washington University in St. Louis, St. Louis, MO, USA

[d]Department of Neuroscience, Washington University School of Medicine, St. Louis, MO, USA

[e]Department of Biomedical Engineering, Washington University in St. Louis, St. Louis, MO, USA

[f]VISN17 Center of Excellence for Research on Returning War Veterans, Waco, TX, USA

[g]Department of Neuroscience, University of Padua, Padua, Italy

Abstract

Studies of stroke have identified local reorganization in perilesional tissue. However, because the brain is highly networked, strokes also broadly alter the brain's global network organization. Here, we assess brain network structure longitudinally in adult stroke patients using resting state fMRI. The topology and boundaries of cortical regions remain grossly unchanged across recovery. In contrast, the modularity of brain systems i.e. the degree of integration within and segregation between networks, was significantly reduced sub-acutely ($n = 107$), but partially recovered by 3 months ($n = 85$), and 1 year ($n = 67$). Importantly, network recovery correlated with recovery from language, spatial memory, and attention deficits, but not motor or visual deficits. Finally, in-depth single subject analyses were conducted using tools for visualization of changes in brain networks over time. This exploration indicated that changes in modularity during successful recovery reflect specific alterations in the relationships between different networks. For example, in a patient with left temporo-parietal stroke and severe aphasia, sub-acute loss of modularity reflected loss of association between frontal and temporo-parietal regions bi-hemispherically across multiple modules. These long-distance connections then returned over time, paralleling aphasia recovery. This work establishes the potential importance of normalization of large-scale modular brain systems in stroke recovery.

Corresponding author. Washington University School of Medicine, Department of Neurology 4525 Scott Ave, Rm 2127 St. Louis, MO 63110, USA. jssiegel@wustl.edu (J.S. Siegel).

1. Introduction

The human brain is a collection of widely distributed cortical and sub-cortical systems that flexibly interact to enable cognitive function. The analysis of temporally correlated spontaneous activity, measured in the resting state with the blood oxygenation level dependent (BOLD) signal, has emerged as a powerful tool for mapping brain network connectivity (Fox et al., 2005). resting state functional magnetic resonance imaging (R-fMRI) studies have defined hierarchical and distributed brain networks (Power et al., 2011; Yeo et al., 2011) that correspond to the brain's functional domains (Bertolero, Yeo, & D'Esposito, 2015; Smith et al., 2009). The spatial and temporal features of this organization appear to be optimized to support the segregation and integration of information (Petersen & Sporns, 2015).

A major goal in the study of stroke is to understand how stroke affects these distributed brain networks. Although structural damage from stroke is focal, remote perturbations occur in regions of the brain distant from the area of damage (Carrera & Tononi, 2014). The set of regions that are directly damaged or indirectly affected is in turn embedded within a larger functional system that is in dynamic balance with other systems in the brain (Corbetta, 2012). In prior work, we have shown that R-fMRI can be used to identify broad patterns of functional connectivity disruption that correspond to numerous behavioral deficits after stroke (Siegel, Mitra, et al., 2016).

The healthy brain demonstrates integration within functional systems – measurable as highly correlated resting BOLD signals within systems – as well as segregation between systems – measurable as low correlations in resting BOLD signals across systems. This network property can be quantified with Modularity – a global network measure that compares the density of connections inside communities to the connections between communities (Newman, 2004). Modular brain architecture is thought to enable efficient processing and flow of information (Bullmore & Sporns, 2009). Studies of aging and disease have provided evidence for the important of modular brain systems to cognitive function (for a review, see Wig, 2017).

In contrast with the healthy brain, a common phenotype of stroke is a reduction of inter-hemispheric homotopic integration, and a reduction of within-hemisphere segregation between different brain systems (Siegel, Mitra, et al., 2016). Both of these changes are consistent with a reduction in network modularity, which has been observed in stroke patients, even in the unaffected hemisphere (Gratton, Nomura, Pérez, & D'Esposito, 2012). A recent study of aphasia patients found that improved narrative production following therapy correlated with an improvement in modularity of resting state networks (Duncan & Small, 2016).

In the months following stroke, patients typically recover between 40 and 70% of initial clinical deficit (Lazar & Antoniello, 2008; Prabhakaran et al., 2007; Ramsey et al., 2017). Evidence for functional remapping of sensory and motor function has been observed within a few millimeters of lesion boundaries (Murphy & Corbett, 2009; Nudo & Milliken, 1996). Normalization of connectivity with sites distant from the lesion has been observed in parallel with recovery (He et al., 2007; Lim, LeDue, Mohajerani, & Murphy, 2014; Ramsey et al., 2016; van Meer et al., 2010). Little is known about how brain networks change on a larger spatial and temporal scale after stroke, and the behavioral relevance of both local and global changes remains unclear.

In the present work, we relate deficit and recovery following stroke to disruptions of the modular organization of brain systems. Specifically, we hypothesize that brain systems become less modular following stroke and that recovery of deficit can be predicted by the return of modularity. To test this, we follow a large prospective cohort of stroke patients over the course of deficit and chronic recovery – acquiring R-fMRI, and neuropsychological assessment at two weeks, three months, and one-year post-stroke.

2.   Materials & methods

2.1.   Subject enrollment & retention

Written informed consent was obtained from all participants in accordance with the Declaration of Helsinki ND procedures established by the Washington University in Saint Louis Institutional Review Board. All participants were compensated for their time. All aspects of this study were approved by the Washington University School of Medicine (WUSM) Internal Review Board.

First time human stroke patients with clinical evidence of motor, language, attention, visual, or memory deficits based on neurological examination were included. 132 patients met all inclusion criteria and completed the entire sub-acute protocol (mean age 52.8 years with range 22–77, 119 right handed, 63 female, 64 right hemisphere). Patients were excluded from analysis for poor quality imaging data (n = 5), hemodynamic lags >1 sec on average between hemispheres (n = 6), and less than 180 frames remaining after motion scrubbing (n = 15), leaving 107 subjects in the final analysis (Table 1).

A second timepoint occurred 3 months post-stroke. Some patients were lost due to recurrent stroke/other neurological problems (n = 5), not well enough to participate (n = 5), refused to participate (n = 7), moved away (n = 1), or no response to multiple contact attempts (n = 11), resulting in 103 patients completing the protocol at 3 months. In addition, patients were excluded based on imaging quality (n = 7), lags >1 sec (n = 4), and <180 R-fMRI frames (n = 7), leaving 85 subjects in the final analysis (Table 1).

A third timepoint occurred 1 year post-stroke. Three patients returned after missing timepoint 2. Others were lost due to recurrent stroke/other neurological problems (n = 4), not well enough to participate (n = 5), refused to participate (n = 1), moved away (n = 1), or no response to multiple contact attempts (n = 7), resulting in 88 patients completing the protocol at 1 year. In addition, patients were excluded based on imaging quality (n = 7), lags

>1 sec (n = 5), and <180 R-fMRI frames (n = 9), leaving 67 subjects in the final analysis (Table 1).

There was no difference in behavioral scores in any domains reported between those patients that returned for follow up at 1 year and those lost to follow-up or data exclusion criteria (Language: $t_{(122)} = 1.18$, $p = .24$; Left Motor: $t_{(115)} = 1.00$, $p = .32$; Right Motor: $t_{(115)} = .40$, $p = .69$; Attention $t_{(99)} = -.50$, $p = .62$).

Demographically matched controls (n = 30) were recruited and underwent the same behavioral and imaging exams (mean age 55.7 years, SD = 11.5, range 21–83). Controls were matched to the study population in age, gender, handedness, and level of education. Controls were excluded based on lags (n = 1 at TP1, n = 1 at TP2), and <180 R-fMRI frames (n = 3 at TP1, n = 4 at TP2), leaving 26 controls at timepoint 1 and 25 controls at timepoint 2 (Table 1).

2.2. Neuropsychological evaluation

Participants underwent a behavioral battery that included several assessments of motor, language, attention, memory, and visual function following each scanning session. The specific measures are described in detail in Siegel, Mitra, et al. (2016) (Supplementary methods). Briefly, they included the following: MOTOR-Active Range Of Motion, Jamar Dynamometer, nine-hole peg test, Action Research Arm Test, motricity index, and Functional Independence Measures walk test; LANGUAGE-Boston Diagnostic Aphasia Examination, nonword reading, stem completion, and animal naming; ATTENTION-Posner visual orienting task, Mesulam symbol cancellation test, and Behavioral Inattention Test Star Cancellation; MEMORY-Brief Visuospatial Memory Test, Hopkin's Verbal Learning Test, and spatial span; VISUAL-computerized perimetry.

Imaging and behavioral testing sessions were usually performed on the same day. Scores were only recorded for tasks that subjects were able to complete. Dimensionality reduction was performed on the performance data using principal component analysis as described in detail in (Corbetta et al., 2015). Briefly, tasks were first categorized as attention, language, memory, motor, and vision. Next, a principal components analysis (PCA) was run on each category and the first component was used as a domain score. The attention score was correlated with measures of attentional field bias such as the Mesulam center of cancellation score (r = .749) and the visual field effect in the Posner task (r = .828). The language score was correlated with measures of word comprehension (r = .858), complex ideational material (r = .885), and object naming (r = .925). In the memory domain, the first two components were used (named 'Spatial Memory' and 'Verbal Memory') because the first component was correlated with measures of visuospatial memory such as delayed recall of visual information on the Brief Visuospatial Memory Test (r = .81) and the second was correlated with measures of verbal memory such as delayed recall of words on the Hopkins Verbal Learning Test (r = .93). In the motor domain, the first two components correlated with left and right motor function. The left motor score correlated with left shoulder flexion (r = .947), left hand 9-hole peg test (r = .850), and left lower extremity motricity index (r = .917). The right motor score correlated with right shoulder flexion (r = .893), right hand 9-hole peg test (r = .825), and right lower extremity motricity index (r = .896). In stroke

patients, a single motor score assessing contralesional deficit (contralesional motor minus ipsilesional motor) was used for comparison to modularity. For the complete list of tests used and correlations with the factor scores, see Corbetta et al., 2015.

Visual field deficits were measured using a computerized perimeter (Humphrey Field Analysis Model 750i). Each eye was tested using the central 24–2 threshold SITA-FAST protocol. PCA was not done because vision was assessed with a single functional test. Instead, the mean pattern deviation scores in the left and right hemifields determined left and right vision scores, respectively. As with motor, a single visual score was generated by subtracting ipsilesional pattern deviation from contralesional pattern deviation.

Behavioral scores at chronic timepoints were calculated using the factors defined at the sub-acute timepoint. Scores in each domain were continuous and were normalized to have a mean of 0 and standard deviation of 1 in controls, with lower scores indicating a greater deficit. In each domain, 'Good recovery' was defined as a change of >2SD between 2 weeks and 1 year; 'No recovery' was defined as a change of <1SD. Scores for each timepoint in every patient and in every domain, are shown in Fig. S1.

2.3. Imaging

Patients were studied two weeks (mean = 13.4 days, SD = 4.8 days), three months (mean = 112.5 days, SD = 18.4 days), and one year (mean = 393.5 days, SD = 55.1 days) after stroke onset. Controls were studied twice at an interval of 3-months. All imaging was performed using a Siemens 3T Tim-Trio scanner at the Washington University School of Medicine (WUSM) and a standard 12-channel head coil. The MRI protocol included structural, functional, pulsed arterial spin labeling (PASL), and diffusion tensor scans. Structural scans included: (1) a sagittal T1-weighted MP-RAGE (TR = 1950 msec, TE = 2.26 msec, flip angle = 90°, voxel size = $1.0 \times 1.0 \times 1.0$ mm); (2) a transverse T2-weighted turbo spin-echo (TR = 2500 msec, TE = 43 msec, voxel-size = $1.0 \times 1.0 \times 1.0$ mm); and (3) sagittal FLAIR (fluid attenuated inversion recovery) (TR = 750 msec, TE = 32 msec, voxel-size = $1.5 \times 1.5 \times 1.5$ mm). Resting state functional scans were acquired with a gradient echo EPI sequence (TR = 200 msec, TE = 2 msec, 32 contiguous 4 mm slices, 4×4 mm in-plane resolution) during which participants were instructed to fixate on a small white cross centered on a screen with a black background in a low luminance environment. Six to eight resting state fMRI runs, each including 128 volumes (30 min total), were acquired. A camera fixated on the eyes was used to determine when a subject's eyes were open or closed during scans. Patients had eyes open on 65.6 ± 31.9% of frames, and controls had eyes open on 76.8 ± 30.2% of frames ($t_{(114)} = -1.7$, $p = .091$). Diffusion tensor scans included multi-directional and multi-weighted (64 directions, b value of 1500 sec/mm^2) diffusion weighted images (TR = 9200 ms, TE = 90 ms, 2.0 mm isotropic voxels), requiring 14 min in total.

2.4. Lesion masking

Lesions were manually segmented on individual structural MRI images (T1-weighted MP-RAGE, T2-weighted spin echo images, and FLAIR images obtained 1–3 weeks post-stroke) using the Analyze biomedical imaging software system (www.mayo.edu; Robb & Hanson, 1991). Two board-certified neurologists (Maurizio Corbetta and Alexandre Carter) reviewed

all segmentations. In hemorrhagic strokes, edema was included in the lesion. A neurologist (MC) reviewed all segmentations a second time paying special attention to the borders of the lesions and degree of white matter disease. Atlas-registered segmented lesions ranged from .02 cm^3 to 82.97 cm^3 with a mean of 10.15 cm^3 (SD = 13.94 cm^3). Lesions were summed to display the number of patients with structural damage for each voxel (Fig. 1A).

2.5. fMRI data preprocessing

Preprocessing of fMRI data included: 1) compensation for asynchronous slice acquisition using sinc interpolation; 2) elimination of odd/even slice intensity differences resulting from interleaved acquisition; 3) whole brain intensity normalization to achieve a mode value of 1000; 4) removal of distortion using synthetic field map estimation and spatial realignment within and across fMRI runs; 5) resampling to 3 mm cubic voxels in atlas space including realignment and atlas transformation in one resampling step. Cross-modal (e.g., T2-weighted to T1-weighted) image registration was accomplished by aligning image gradients. Cross-modal image registration in patients was checked by comparing the optimized voxel similarity measure to the 97.5 percentile obtained in the control group. In some cases, structural images were substituted across sessions to improve the quality of registration.

2.6. Functional connectivity processing

Following cross-modal registration, data were passed through several additional preprocessing steps: (i) tissue-based regressors were computed based on FreeSurfer segmentation (Fischl, Sereno, Tootell, & Dale, 1999); (ii) removal by regression of the following sources of spurious variance: (a) six parameters obtained by rigid body correction of head motion, (b) the signal averaged over the whole brain, (c) signal from ventricles and CSF, and (d) signal from white matter; (ii) temporal filtering retaining frequencies in the .009–.08-Hz band; and (iii) frame censoring. The first four frames of each BOLD run were excluded. Frame censoring was implemented using framewise displacement (Power et al., 2014) with a threshold of .5 mm. This frame-censoring criterion was uniformly applied to all R-fMRI data (patients and controls) before functional connectivity computations.

FC quality-based exclusion criteria included 1) less than 180 usable frames after motion scrubbing, and 2) severe hemodynamic lags (greater than 1 sec inter-hemispheric difference) measured from R-fMRI (Siegel, Snyder, et al., 2016). After motion and lag exclusion, 107 patients were included at two weeks, 85 patients at three months, 67 patients at 1 year, 26 controls at timepoint one, and 25 at timepoint two (Table 1).

2.7. Surface processing

Surface generation and processing of functional data followed procedures similar to Glasser et al. (2013), with additional consideration for cortical segmentation in stroke patients. First, anatomical surfaces were generated for each subject's T1 MRI using FreeSurfer automated segmentation (Fischl et al., 1999). This included brain extraction, segmentation, generation of white matter and pial surface, inflation of the surfaces to a sphere, and surface shape-based spherical registration to the subject's "native" surface to the fs_average surface. Segmentations were manually checked for accuracy. For patients in whom the stroke disrupted automated segmentation, or registration, values within lesioned voxels were filled

with normal atlas values prior to segmentation, and then masked immediately after (7 patients). The left and right hemispheres were then resampled to 164,000 vertices and registered to each other (Van Essen et al., 2001), and finally down-sampled to 10,242 vertices each (a combined total of 18,722 vertices after exclusion of the medial wall) for projection of functional data.

Following preprocessing, BOLD data were sampled to each subject's individual surface (between white matter and pial surface) using a ribbon-constrained sampling available in Connectome Workbench (Marcus et al., 2013). Voxels with a high coefficient of variation (.5 standard deviations above the mean coefficient of variation of all voxels in a 5 mm sigma Gaussian neighborhood) were excluded from volume to surface mapping (Glasser et al., 2013). Timecourses were then smoothed along the 10,242 vertex surface using a 3 mm FWHM Gaussian kernel.

All brain surface visualizations were generated using Connectome Workbench (Marcus et al., 2013).

2.8. Gordon & Laumann parcellation

We used a cortical surface parcellation generated by Gordon & Laumann and colleagues (Gordon et al., 2016) (Fig. 1). The parcellation is based on R-fMRI boundary mapping and achieves full cortical coverage and optimal region homogeneity. The parcellation includes 324 regions of interest (159 left hemisphere, 165 right hemisphere). Note that the original parcellation includes 333 regions, while here all regions less than 20 vertices (approx. 50 mm^2) were excluded. This cutoff was arbitrarily chosen based on the assumption that parcels below this size would have unreliable signal given 4 mm sampling of our functional data. Notably, the parcellation was generated on 120 young adults age 18–33 and is applied here to adults age 21–83.

To generate parcel-wise connectivity matrices, time-courses of all vertices within a parcel were averaged. Functional connectivity (FC) was then computed between each parcel timeseries using Fisher z-transformed Pearson correlation. All vertices that fell within the lesion were masked out, and parcels with greater than 50% lesion overlap were excluded from all analyses.

2.9. Parcel homogeneity

Prior to homogeneity analysis, whole-brain connectivity was computed between every pair of vertices (18,722 × 18,722). Next, the following steps were taken to measure parcellation homogeneity. 1) For each parcel, a principal component analysis was run across the connectivity maps of all vertices belonging to that parcel. Parcels contained between 23 and 233 vertices – each first principal component is a connectivity map that explains X% of variance across those vertices. 2) The percent of variance explained by the first principal component was used as a measure of parcel homogeneity. 3) This measured was averaged across all 324 brain parcels to produce a brain-wide measure of parcel homogeneity. 4) To compare this measure to a null distribution (Gordon et al., 2016), the full parcellation was rotated randomly around the cortical surface (1,000 times for the group average FC

homogeneity, 100 times for each individual subject). 5) Parcel homogeneity was reassessed in the same manner using the randomly rotated parcels.

For the group analysis, parcel homogeneity was expressed as a *p*-value based on the number of null rotations with greater homogeneity than the real parcellation. For the individual subject analyses, parcel homogeneity was turned in to a z-score (difference from the mean of the null rotations divided by the standard deviation of the null rotations). Parcels overlapping with the lesion were excluded from the real and null homogeneity. Values were imputed for parcels overlapping the lesion, medial wall, and high susceptibility areas (those colored gray in Fig. 1B) after null rotations.

2.10. FC similarity

To measure similarity between each cohort and controls (at timepoint 1), we developed a simple measure of FC similarity. This measure was computed by turning the 324-by-324 FC matrix into a 52,326 vector for each subject. For a given group (i.e. patients at 2 weeks), a spatial correlation was run between the FC vector of every subject in that group and the FC vector of every subject in the control timepoint 1 group. This generated a distribution of similarity values for each group relative to controls.

2.11. Modularity

Modularity (Newman's Q) was calculated using the equation given in (Newman, 2004)

$$Q \; = \; \sum_{\mu \, \in \, M} \left[e_{uu} - \left(\sum_{v \, \in \, M} e_{uv} \right)^{2} \right] \quad (1)$$

where the network (including nodes and binary undirected links) is fully subdivided into a set of nonoverlapping modules M, and e_{uv} is the proportion of all links that connect nodes in module μ with nodes in module v. Matlab code to calculate modularity and other graph measures (below) was taken from the Brain Connectivity Toolbox (Rubinov & Sporns, 2010), publicly available at sites google.com/site/bctnet/.

Modules assignments were chosen *a priori* based on Info-Map community detection in healthy young adults (Gordon et al., 2016). Parcels with greater than 50% damage due to stroke were removed completely from networks prior to calculating modularity. Modularity was calculated at edge densities ranging from 4% to 20%. This is the range between which modularity was found to be reduced in prior stroke FC analyses (Gratton et al., 2012).

We chose to assess modularity using *a priori* systems rather than systems defined individually using community detection for a number of reasons: 1) we would be measuring modularity in a community structure that has been optimized to increase modularity, thereby making Q a biased statistic, 2) the number of communities found by modularity optimization can vary, and 3) highly localized clusters may appear modular, though they may in reality be attributed to absence of synchronized BOLD fluctuations across distributed brain systems (and thus, predominance of distance dependent influences on the BOLD signal).

Modularity was found to correlate with magnitude of hemodynamic lags (r = 0.374, $p = 7 \times 10^{-5}$), number of frames remaining after scrubbing (r = .316, $p = 9 \times 10^{-4}$), and RMS head motion after scrubbing (r = .279, $p = .0036$). At each edge density, modularity estimates from all subjects at all timepoints were concatenated in to a single vector, and the three confounds were simultaneously regressed out. After confound regression, no significant association remainedbetween any group and any confound measure at any edge density threshold.

Modularity was also measured within each hemisphere. Brainstem stroke patients were excluded from this analysis (as some projection tracts may have crossed the midline), and cerebellar strokes were flipped (i.e. for a right cerebellar stroke, the left cerebral cortex is ipsilesional) based on known cerebro-cerebellar connectivity (Schmahmann & Pandya, 1997). For comparison, control subject hemispheres were randomly labeled ipsilesional or contralesional. Modularity differences were assessed with t-tests for differences between groups (un-paired Student t-test) and across time (paired Student t-test) and tested for significance against a corrected $\alpha = .0063$ corrected for eight comparisons.

In a supplemental analysis, two other global graph measures, small-worldness and Global Efficiency, were measured and compared between groups and over the course of recovery using exactly the same data processing steps as described above for modularity (including controlling for motion and hemodynamic lags). Both were implemented using the brain connectivity toolbox (Rubinov & Sporns, 2010).

To compare modularity with behavioral measures across three timepoints, we first attained a single summary measure of modularity (across edge densities). Modularity values were normalized to average values in controls at each edge density (to have a mean = 1 and SD = .15), and then averaged across edge densities. Next, we modeled change in modularity in each patient. Because stroke recovery is nonlinear, modularity at three timepoints was modeled in each subject using a log function (Suzuki et al., 2013):

$$Y = m * \log(t) + b \quad (2)$$

where t is time post-stroke in days (14, 90, 365) and Y is modularity at each timepoints (Figure S1). The slope m and intercept b were then solved using a least-squares fit. Finally, the slope of modularity recovery was compared between patients who showed good behavioral recovery and those who showed less recovery (defined above) using unpaired t-tests. p-values were False Discovery Rate (FDR) corrected for six comparisons (Benjamini & Hochberg, 1995).

Additional analyses were done comparing sub-acute modularity versus behavior and modularity recovery (slope m) versus behavioral recovery using linear correlation across all subjects so that all data points could be shown. Finally, an additional subgroup analysis was performed to assess modularity recovery versus behavioral recovery in only those patients with sub-acute deficit (>2SD below control mean) in each domain. Patients were categorized as recovery>50% or <50%. 50% is a reasonable approximation of the median recovery

across domains by one year (Ramsey et al., 2017). Because the number of subjects with sub-acute deficit in any given domain was limited, we used a paired t-test to compare average modularity change in good versus poor recovery groups across the four cognitive domains (attention, s. memory, v. memory, language).

2.12. Small-worldness and global efficiency

For comparison, we explored two additional global graph measures: global efficiency and small-worldness. As described for modularity above, both were calculated on binary undirected FC graphs, and both were corrected for head motion and hemodynamic lag. Global efficiency was calculated using the previously published equation (Latora & Marchiori, 2001),

$$E = \frac{1}{n} \sum_{i \in N} \left[\frac{\sum_{j = N} d_{ij}^{-1}}{n - 1} \right] \quad (3)$$

where N is the set of all nodes in the network, n is the number of nodes, and where d_{ij} is the shortest path between nodes i and j. Thus, global efficiency is equal to the average of the inverse of shortest path length between all node pairs.

Small-worldness was calculated using the previously published equation (Watts & Strogatz, 1998),

$$S = \frac{C/C_{\text{rand}}}{L/L_{\text{rand}}} \quad (4)$$

where C is the clustering coefficients, L is the characteristic path lengths, and $C_{rand}$are and L_{rand} are the same measures calculated on random networks with equal edge density. Clustering coefficient is the fraction of nodes neighbors that are also connected to each other. Characteristic path length is inverse of global efficiency, so d_{ij}^{-1} (equation (3)) is replaces with d_{ij}. See Rubinov & Sporns (2010) for the complete equations for clustering coefficient and characteristic path length.

In addition, we measured small-world propensity; a variation on the small-worldness measure that has been adapted to be used on weighted graphs (Muldoon, Bridgeford, & Bassett, 2016). Specifically, we first thresholded at 40% edge density to avoid negative weights, and then used the Onnela approach for measuring clustering in weighted networks (Onnela, Saramäki, Kertész, & Kaski, 2005).

2.13. Controlling for lesioned nodes in modularity analysis

As a control analysis, lesion masks from the stroke patients were used to remove nodes in age-matched controls and modularity was calculated. This was done by identifying excluded nodes in all patients, and then excluding those same nodes from age-matched controls and measuring modularity on the resulting FC matrix. For example, if 13 parcels were excluded

due to damage (as is the case in Subject 108 in Fig. 5), then those same 13 nodes would be removed from the 280 network-assigned nodes in a control, leaving a 267×267 FC matrix with which to calculate modularity. Because there are far more stroke patients than age-matched controls, controls were replicated 4–5 times in order to produce a 'controls (minus lesion nodes)' group with the same number of subjects and distribution of lesions as the patients.

2.14. Spring-embedding

Network structure for each subject was visualized using spring-embedded plots. The 324 parcel FC matrix was thresholded at 4% edge density. Connections act as "springs" between pairs of nodes (parcels) in the spring-embedded plot in order to position nodes in space such that communities are pulled together. Nodes are colored based on the previously defined InfoMap community assignment (Gordon et al., 2016). A spring-embedded representation of a highly modular brain would show tight clustering within communities (nodes of the same color) and wide spacing between communities (Power et al., 2011).

3. Results

3.1. Functional brain areas defined in healthy young adults remain present across stroke and recovery

In this study, we recruited 132 stroke patients with heterogeneous lesions (Fig. 1A) using MRI, R-fMRI, and neuropsychological evaluation. After careful censoring for motion and hemodynamic lags, data at two weeks (n = 107), three months (n = 85), and one year (n = 67) were investigated and compared to controls at two timepoints (n = 26 & n = 25). We first asked whether brain areas and areal boundaries remain constant in stroke patients. Of note, these questions were posed with respect to gross changes occurring throughout the cortex and should be thought of as complementary to studies of remapping that have focused with high resolution on perilesional cortex. We applied a cortical parcellation developed on an independent sample of 120 healthy young adults (mean age 25, range 19–31) (Fig. 1B: Gordon et al., 2016) to R-fMRI data from 107 stroke patients (mean age 53, range 22–77) and 26 demographically matched controls (mean age 56, range 21–83). To determine if the cortical parcellation could accurately define functional brain areas and areal boundaries in our patients and controls, parcel homogeneity was assessed (Gordon et al., 2016). Briefly, for a parcel, the brain-wide connectivity pattern of all vertices was entered into a principal component analysis (PCA). Parcel homogeneity was determined as the percent of variance in connectivity across all vertices explained by the first principal component. Mean parcel homogeneity was determined by averaging homogeneity values across all parcels. To determine parcellation fit, real mean parcel homogeneity was compared to the mean homogeneity values from 1,000 randomly rotated null model parcellations.

Mean parcel homogeneity in age-matched control subjects was 76.7% and in sub-acute stroke patients was 75.1%. In both cohorts, the 324-region cortical parcellation yielded higher average parcel homogeneity than all 1,000 null rotations (Fig. 1D). These results indicate that cortical areas and the boundaries between areas remain largely constant in aging adults and even following stroke. Both real and null group-averaged parcel

homogeneity were slightly lower in patients than controls. This may suggest a greater degree of heterogeneity of connectivity in patients in general.

The same procedure was then conducted on individual subjects. Fig. 1E illustrates the relative homogeneity (average real homogeneity minus average null parcel homogeneity) for each subject at each timepoint. In all cohorts at all timepoints, parcel homogeneity was significantly greater than null. No significant difference was observed between groups or time-points. Nevertheless, a correlation was observed between lesion size and parcel homogeneity (Spearman's $\rho = -.266$, $p = .009$). Parcel homogeneity scores were similar between two weeks and three months in patients (Pearson's r = .58, $p = 2.9 \times 10^{-7}$), and across timepoints in controls (Pearson's r = .62, $p = .002$). From this set of analyses, we concluded that the parcellation provides a reasonable representation of cortical areas in the majority of individual subjects, and that cortical areas remain largely stable over the course of stroke recovery.

Community structure in both patients and controls remained qualitatively similar to community structure described using the InfoMap algorithm in healthy young adults by (Gordon et al., 2016) (Fig. 1C). Looking broadly at FC, we found that functional connectivity tends to normalize (became more similar to controls) over recovery (Fig. 2). At the sub-acute timepoint (red curve), FC was least similar to control subjects. Over recovery, patient FC became more similar to controls, and less heterogeneous (orange and green curves).

3.2. Modularity is reduced sub-acutely but returns in parallel with behavior

Having validated the use of the 324-region cortical parcellation, we next investigated our central question: how does network modularity change following stroke? Modularity is calculated on binary graphs (Fig. 3A), whereas functional connectivity values are continuous (z-transformed Pearson correlation coefficient). Thus, we thresholded each subject's connectivity matrix at a range of edge densities (between 4% and 20%), and calculated modularity (as defined in equation (1)). We found that modularity in patients was significantly lower than controls two weeks after stroke (Fig. 3B), indicating a reduction in segregation of resting state networks. This relationship was present despite correcting for subject motion and hemodynamic lags (Siegel, Ramsey, et al., 2016). Over the course of stroke recovery, modularity increased towards the level of controls (Fig. 3C). In Fig. 3D and for subsequent analyses, modularity values were normalized and then averaged across edge densities such that controls had a mean of 1 and standard deviation of .15.

Across the whole brain, the majority of modularity increase during stroke recovery came between two weeks and three months (average normalized modularity .83 to .91; paired t-tests, Bonferonni corrected $\alpha = .0063$; $t_{(73)} = -4.0$, $p = 6.3 \times 10^{-5}$). There was no significant change between 3 months and one year (.91–.92; $t_{(60)} = -.19$, $p = .43$). Both ipsilesional and contralesional hemispheres showed an initial decrease in within-hemisphere modularity, but the decrease was larger in the ipsilesional than the contralesional hemisphere (.81 *vs* .93). The ipsilesional hemisphere showed a significant increase from two weeks to three months (Q = .81, .88; $t_{(65)} = -3.7$, $p = 2.3 \times 10^{-4}$), while the contralesional hemisphere did not change significantly (Q = .93, .96; t(65) = −2.3, p = .011) (Fig. 3D).

In patients, there was a significant correlation between lesion size and modularity at two weeks (r = −.27, p = .0052), and at three months (r = −.22 p = .048), but not at one year (r = −.01, p = .91). A relationship also existed between lesion size and change in modularity between two weeks and one year (r = .37, p = .0047). To confirm that the observed modularity decrease in stroke was not trivially caused by exclusion of lesioned nodes, we masked the same nodes in controls. Masking equivalent nodes did not significantly change modularity in controls (Fig. 3D). Furthermore, number of nodes removed in controls did not correlate with modularity (r = .03, p = .73). Additionally, there was no significant correlation between percent of frames with eyes open and modularity in patients (r = .09, p = .42).

Next, we investigated the relationship between modularity and cognitive function. To test this, we assessed function in six domains: 1) spatial attention – assessing visual attention to the contralesional hemifield, 2) spatial memory, 3) verbal memory, 4) language – including both receptive and productive measures 5) contralesional motor – including a composite of upper and lower limb function and 6) contralesional visual field. Consistent with prior reports (Lazar & Antoniello, 2008; Prabhakaran et al., 2007; Ramsey et al., 2017), the majority of clinical recovery occurred in the first three months, with small additional improvement by 1 year (Fig. S1).

To determine if a relationship was present between recovery of behavior and recovery of modularity, we first defined a 'good recovery' and a 'no recovery' group in each behavioral domain. 'Good recovery' patients were those whose behavior score increased by >2SD between 2 weeks and 1 year. 'No recovery' patients were those whose behavior score increased by <1SD in that same period (note that this includes patients without initial deficit). Next, we tested if there was a difference in modularity change between the two groups.

In multiple behavioral domains, good recovery was paralleled by a return of brain network modularity (Fig. 4). Specifically, good recovery from deficits in attention, spatial memory, and language were all associated with a greater increase in modularity (attention p_{DFR} = .0365; spatial memory p_{DFR} = .0369; language p_{DFR} = .0365). By contrast, in motor and visual domains, recovery was not associated with a greater change in whole brain modularity (motor p_{DFR} = .1471; visual p_{DFR} = .1645). In the verbal memory domain, there was a trend towards greater modularity increase in the good recovery group (p_{FDR} = .0947). Behavior-modularity relationships remained present when recovery of deficit was compared to recovery of modularity across patients using linear correlation (Fig. S2). Relationships were weaker in all cognitive domains (attention, memory, language) when change in behavior was compared to modularity in either hemisphere alone (Fig. S2C–D).

In a supplemental analysis, we tested the hypothesis that good recovery paralleled a return of brain network modularity when controlling for sub-acute deficit. Because the number of subjects with sub-acute deficit in any single domain was limited, we compared average modularity change in good (>50% of initial deficit) versus poor (<50%) recovery groups across the four cognitive domains. In all domains, groups did not differ in initial deficit (Fig. S3A; two-tailed t-test, $p_{uncorrected}$>.05). Good recovery of cognitive deficits (attention, v. memory, s. memory, language) corresponded to a larger increase in modularity than poor

recovery (Fig. S3B; paired t-test of average modularity changes in cognitive recovery groups; $p = .0075$).

Newman's modularity can also be formulated for weighted graphs. To confirm that the use of binary graphs did not affect the observed results, analyses were repeated using weighted graphs. However, the weighted modularity equation cannot accommodate anti-correlations, thus we used a hybrid in which edges below a given edge density were set to zero. Longitudinal changes in modularity as well as associations between behavioral recovery and recovery of brain network modularity remained unchanged when weighted graphs were used (Fig S4).

Previous work identified reduced homotopic integration and reduced within-hemisphere segregation as important and related phenotypes of stroke (Siegel, Ramsey, et al., 2016). We conducted additional analyses to determine how the global measure of modularity relates to homotopic FC and ipsilesional dorsal attention network (DAN)– default mode network (DMN) FC (known to be strongly anti-correlated in the healthy brain). We found that modularity in patients correlated with both homotopic connectivity (r = .45, $p = 9.9 \times 10^{-6}$) and with ipsilesional DAN–DMN FC (r = −.38, $p = 2.9 \times 10^{-4}$) at 2 weeks. However, when both of these FC measures were regressed out from modularity in patients and controls, modularity still showed a significant increase over time (Fig. S5). This suggests that reported changes in brain network modularity are partially but not entirely related to prior studies associating homotopic FC and contralesional DAN–DMN FC with recovery of neglect (Ramsey et al., 2016).

3.3. Visualizing recovery of the brain graph in single patients

Modularity is a brain-wide measure that cannot provide insight into what is happening at the level of individual brain areas or brain systems. Thus, to gain insight into how the strength of connections within and between systems is changing as modularity returns, we visualized local 'FC variance' as well as spring-embedded graphs in a series of three single case studies.

Patient 108 (P108) suffered a large stroke to the left parietal and temporal lobes (Fig. 5), resulting in severe aphasia, with performance 11.7 standard deviations below control average. The patient recovered to 2.3 standard deviations below controls by 3 months, and showed a small additional improvement (to within 2 standard deviation) by 1 year post-stroke. The patient's modularity score was .66 at 2 weeks (control mean = 1, SD = .15), and had increased to 1.0 by 3 months.

Fig. 5 illustrates the re-emergence and re-segregation of brain systems over the course of recovery in P108 (relative to controls in the right column). The top row shows 'FC variance' – the squared standard deviation of all within-hemisphere correlation coefficients greater than 20 mm from the seed. A normally functioning area will show strong positive FC within system and negative FC with other systems, resulting in high FC variance (as is seen in the control average in the right column) relative to a non-functional area. Thus, FC variance reasonably assays integration within a brain system and segregation between brain systems.

The bottom row shows brain networks visualized as a spring-embedded graph. In the spring-embedded graphs, nodes represent brain parcels and are colored based on their RSN membership (defined in Fig. 1), and edges reflect connections between nodes. The spring-embedded graphs make it possible to visualize the 'distance' (in the graph-theoretical sense) between brain systems. At 2 weeks, systems that are normally highly segregated are clustered together (e.g., the somato-motor and default mode networks, indicated by cyan and red ovals, respectively). Over recovery, the integration within brain systems does not appear to change, but segregation between brain systems increases. The somato-motor and default mode systems become more segregated (e.g., the distance between the cyan and red ovals increases over recovery, becoming more similar to controls). Together, the different visualizations in Fig. 5 provide a picture of acute loss and chronic return of distributed and segregated brain systems in an individual brain.

In Figs. 6 and 7, the same visualizations are shown for two additional subjects. Patient P30 suffered a large MCA stroke to the insula, prefrontal cortex, and underlying white matter (Fig. 6). This patient showed severe left hemi-neglect, poor recovery by one year, and low modularity at all three time-points. At the sub-acute timepoint there is poor integration within and segregation between brain systems. In contrast to P108 (who recovered well), network segregation in P30 remains low across all 3 timepoints. This parallels the patient's poor functional recovery. Patient P161 suffered a large MCA stroke in the caudate, putamen, and insula (Fig. 7). The patient exhibited severe left hemiparesis sub-acutely, but recovered substantially over time (though remained 3.8SD below average). Despite this, the patient showed normal modularity at all timepoints. Modularity was not related to recovery in this patient because the deficit was in motor function rather than higher cognitive functions.

3.4. Comparison to small-worldness and global efficiency

To further quantify changes in the whole brain network after stroke and over recovery, we explored two additional global graph measures: global efficiency and small-worldness. We found that small-worldness in patients was significantly lower than controls two weeks after stroke for edge densities above .05 (Fig. 8A). Over the course of recovery, small-worldness increased towards the level of controls. In contrast to modularity (and behavior), the increase from two weeks to three months was equal or slightly less than the increase between three months and one year. We found that global efficiency did not differ significantly between controls and patients or over recovery (Fig. 8B).

4. Discussion

We assessed longitudinal changes in brain networks after stroke, using R-fMRI. We first established that the topology and boundaries of cortical regions remain grossly unchanged across recovery. Next, we found that brain network modularity was significantly reduced sub-acutely, but partially recovered over time. Reduced modularity reflects both reduced integration within functional brain systems and reduced segregation between systems. Importantly, the return of modular network organization paralleled recovery of language and attention, but was not significantly related to motor or visual recovery. This suggests that

return of efficient processing and flow of information is critical to the return of higher cognitive function.

Remapping and reorganization have been demonstrated as a critical part of adult stroke recovery, but these processes are only observed within a few millimeters of lesion borders and the first month after stroke (Murphy & Corbett, 2009; Nudo & Milliken, 1996; Winship & Murphy, 2009). Our results argue that a normalization of balanced and modular brain systems predominates over a much larger spatial and temporal scale. This is consistent with prior findings of acute decrease and chronic recovery of long-range interhemispheric connections in mice (van Meer et al., 2010) and in humans (Ramsey et al., 2016) paralleling behavioral recovery. The possibility of simultaneous local reorganization and global normalization is supported by mouse models of stroke in which neural activity was measured both globally and locally (1–2 mm from the infarct) using optogenetic photostimulation (Lim et al., 2014). A global scaling (relative decrease) in connectivity occurred acutely, but recovered with time. Whereas, in perilesional tissue, non-uniform changes in connectivity were observed, consistent with remapping. These local and global observations likely reflect two distinct neurobiological processes occurring in the course of stroke recovery.

This work sheds further light on the complex relationship between local damage, global brain connectivity, and behavioral deficit. Prior research has illustrated that lesions to critical white matter locations produce more domain-general deficit (Corbetta et al., 2015) and that lesions to cortical connector 'hubs' produces more profound disruption of global modularity (Gratton et al., 2012) and may lead to more severe deficit (Power, Schlaggar, Lessov-Schlaggar, & Petersen, 2013). A complementary observation is that behavioral deficit after stroke is linked to disruptions in brain connectivity (Carter et al., 2010). But a nuance of this link is that higher cognitive deficits are more strongly linked to FC disruption, whereas motor and visual deficits are less linked by FC (but better predicted by lesion location) (Siegel, Ramsey, et al., 2016). The present results suggest that the healthy brain's modular network organization is critical for higher cognitive functions such as language and attention. The present study further shows that, despite severe disruptions, the post-stroke brain is capable of returning to a state of modular organization in the course of recovery. Interestingly, modularity seems to reflect a unique and important measure of post-stroke disruption, as the initial reduction and later increase of modularity was observed even when homotopic FC was accounted for (Fig S5).

There are multiple global graph measures that could be used to quantify characteristics of the FC-derived brain network. We chose *a priori* to focus on modularity because it unifies two previously observed behaviorally relevant FC changes: reduction of inter-hemispheric homotopic integration, and a reduction of within-hemisphere segregation between different brain systems (Siegel, Ramsey, et al., 2016). However, global efficiency (inverse shortest path length), and small-worldness are two other measures used commonly to describe global properties of graphs (Rubinov & Sporns, 2010). Small-worldness, in particular, has previously been used to describe brain organization (Bassett & Bullmore, 2006). It measures ability to cluster locally (similar to modularity) but also maintain short paths between clusters (similar to efficiency). In our dataset, efficiency did not differ between groups and

small-worldness behaved similarly to modularity, decreasing after stroke and increasing with recovery (Fig. 8). We can thus infer that differences in small-worldness are a result of changes in the numerator (clustering), but not the denominator (average path length) after stroke.

A variety of physiological mechanisms may be responsible for acute disruption and chronic normalization in the synchrony of infra-slow resting BOLD fluctuations. In the period following a stroke, molecular, cellular, and physiological changes occur not only in perilesional tissue, but throughout the brain (Carrera & Tononi, 2014; Feeney & Baron, 1986; Murphy & Corbett, 2009). Further work will be needed to provide a physiological interpretation for reduced network modularity.

Head motion and hemodynamic lags both alter the measurement of modularity in R-fMRI data. Head motion is known to affect FC (Power, Barnes, Snyder, Schlaggar, & Petersen, 2012; Satterthwaite et al., 2012) and impact FC-behavior relationships (Siegel, Mitra, et al., 2016). A number of methods to remove effects of head motion have been described (Power et al., 2014) and benchmarked (Ciric et al., 2016). In line with recommendations, all data in this study were carefully censored (using both head motion and frame-to-frame fMRI signal intensity change (DVAR) thresholds), tissue-based timecourse regression was applied, and potential confounds (FD, frames remaining) were regressed from modularity at the group level. After cleaning and exclusion, patients did not differ from controls on head motion.

The question of how to interpret hemodynamic disruptions is complex. Prior work has noted that lags reflect changes in perfusion (Amemiya, Kunimatsu, Saito, & Ohtomo, 2013; Lv et al., 2013) and correlate with deficit after stroke (Siegel, Mitra, et al., 2016). However, for R-fMRI to best reflect functional connectivity in stroke we hold that hemodynamic lags should be removed (for a review of this issue, see Siegel, Shulman, & Corbetta, 2017). In this work, subjects showing severe hemodynamic disruption (hemodynamic lag >1 sec) were excluded and lag was regressed from modularity in the remaining data. Thus, while both motion and hemodynamic lags are areas of ongoing methods development, we have made a pointed effort to address both confounds to the best of our ability in the present work.

In this work, we assess modularity relative to an *a priori* community structure defined in an independent group of young adults. An alternative approach would be to find community structure in each individual, and then measure modularity. However, such an approach would be less biologically valid and less interpretable for a number of reasons (see Methods: Modularity for a more lengthy consideration). Likewise, using an *a priori* community structure defined on our age-matched controls would bias controls towards greater modularity. An assumption of our approach is that community structure remains largely constant over the course of recovery. We validate this assumption by showing that, over recovery, patterns of brain connectivity become more similar to controls (Fig. 2).

A limitation of this work is that lesion and deficit were heterogeneous in our cohort. Thus, if multiple specific patterns of reorganization were present, these would have been overshadowed by the common trend of normalization. Animal models with controlled lesions (Watson, Dietrich, Busto, Wachtel, & Ginsberg, 1985) are better suited to studying

reorganization, although interventions intended to produce one specific type of reorganization in commonly deficient human cohorts have also shown success (Liepert, Bauder, Miltner, Taub, & Weiller, 2000). An additional limitation is that Newman's modularity cannot factor in effects of negative connections (anti-correlations). Thus, negative FC values are set to zero in binary matrices. The putative role that restoration of anti-correlations plays in recovery (Ramsey et al., 2016) may be downplayed by this approach.

Further, while we controlled for differences in eye condition (open us closed) to the best of our ability, it is possible that systematic differences in eye condition affected our results. Future work may benefit from explicit tests of network differences between eye condition, as it has been shown to affect functional network organization (Laumann et al., 2015).

Here, we observed that modular network structure was reduced after stroke, but recovered over time, in concert with behavioral recovery. Critically, our work suggests that the global normalization of network structure predicts recovery of higher cognitive functions of language and attention, but not motor or visual function. Future studies might therefore also explore how rehabilitation strategies can improve the function of global brain systems thereby promoting across-domain recovery of function.

4.1. Data availability

All data is publicly available through the Central Neuro-imaging Data Archive (https://cnda.wustl.edu/). Data analysis was conducted in matlab, and can be accessed at [analysis code will be posted online prior to publication].

Supplementary Material

Refer to Web version on PubMed Central for supplementary material.

Acknowledgment

Glossary

Glossary

R-fMRI	resting state functional magnetic resonance imaging
BOLD	blood oxygenation level dependent
FC	functional connectivity
DVARS	frame-to-frame fMRI signal intensity change (mean of whole-brain differentiated BOLD time series)

Resting state communities

VIS	visual network
PO	parieto-occipital
SMD	dorsal somato-motor
SMV	ventral somato-motor
AUD	auditory
CON	cingulo-opercular
VAN	ventral attention
SAL	salience
CP	cingulo-parietal
DAN	dorsal attention network
FPN	frontoparietal network
DMN	default mode network
NON	no assigned network

REFERENCES

Amemiya S, Kunimatsu A, Saito N, & Ohtomo K (2013). Cerebral hemodynamic impairment: Assessment with resting-state functional MR imaging. Radiology, 130982 10.1148/radiol. 13130982.

Bassett DS, & Bullmore E (2006). Small-world brain networks. The Neuroscientist, 12(6), 512–523. 10.1177/1073858406293182. [PubMed: 17079517]

Benjamini Y, & Hochberg Y (1995). Controlling the false discovery rate: A practical and powerful approach to multiple testing. Journal of the Royal Statistical Society. Series B (Methodological), 57(1), 289–300.

Bertolero MA, Yeo BTT, & D'Esposito M (2015). The modular and integrative functional architecture of the human brain. Proceedings of the National Academy of Sciences of the United States of America, 112(49), E6798–E6807. 10.1073/pnas.1510619112. [PubMed: 26598686]

Bullmore E, & Sporns O (2009). Complex brain networks: Graph theoretical analysis of structural and functional systems. Nature Reviews Neuroscience, 10(3), 186–198. 10.1038/nrn2575. [PubMed: 19190637]

Carrera E, & Tononi G (2014). Diaschisis: Past, present, future. Brain, 137(9), 2408–2422. 10.1093/brain/awu101. [PubMed: 24871646]

Carter AR, Astafiev SV, Lang CE, Connor LT, Rengachary J, Strube MJ, et al. (2010). Resting interhemispheric functional magnetic resonance imaging connectivity predicts performance after stroke. Annals of Neurology, 67(3), 365–375. 10.1002/ana.21905. [PubMed: 20373348]

Ciric R, Wolf DH, Power JD, Roalf DR, Baum G, Ruparel K, et al. (2016). Benchmarking confound regression strategies for the control of motion artifact in studies of functional connectivity. ArXiv: 1608.03616 [q-Bio]. Retrieved from http://arxiv.org/abs/1608.03616.

Corbetta M (2012). Functional connectivity and neurological recovery. Developmental Psychobiology, 54(3), 239–253. 10.1002/dev.20507. [PubMed: 22415913]

Corbetta M, Ramsey L, Callejas A, Baldassarre A, Hacker CD, Siegel JS, et al. (2015). Common behavioral clusters and subcortical anatomy in stroke. Neuron, 85(5), 927–941. 10.1016/j.neuron. 2015.02.027. [PubMed: 25741721]

Duncan ES, & Small SL (2016). Increased modularity of resting state networks supports improved narrative production in aphasia recovery. Brain Connectivity, 6(7), 524–529. 10.1089/brain. 2016.0437. [PubMed: 27345466]

Feeney DM, & Baron JC (1986). Diaschisis. Stroke, 17(5), 817–830. 10.1161/01.STR.17.5.817. [PubMed: 3532434]

Fischl B, Sereno MI, Tootell RBH, & Dale AM (1999). High-resolution intersubject averaging and a coordinate system for the cortical surface. Human Brain Mapping, 8(4), 272–284. [PubMed: 10619420]

Fox MD, Snyder AZ, Vincent JL, Corbetta M, Van Essen DC, & Raichle ME (2005). The human brain is intrinsically organized into dynamic, anticorrelated functional networks. Proceedings of the National Academy of Sciences of the United States of America, 102(27), 9673–9678. 10.1073/ pnas.0504136102. [PubMed: 15976020]

Glasser MF, Sotiropoulos SN, Wilson JA, Coalson TS, Fischl B, Andersson JL, et al. (2013). The minimal preprocessing pipelines for the Human Connectome Project. Neuroimage, 80, 105–124. 10.1016/j.neuroimage.2013.04.127. [PubMed: 23668970]

Gordon EM, Laumann TO, Adeyemo B, Huckins JF, Kelley WM, & Petersen SE (2016). Generation and Evaluation of a cortical area parcellation from resting-state correlations. Cerebral Cortex (New York, N.Y.: 1991), 26(1), 288–303. 10.1093/cercor/bhu239.

Gratton C, Nomura EM, Pérez F, & D'Esposito M (2012). Focal brain lesions to critical locations cause widespread disruption of the modular organization of the brain. Journal of Cognitive Neuroscience, 24(6), 1275–1285. 10.1162/jocn_a_00222. [PubMed: 22401285]

He BJ, Snyder AZ, Vincent JL, Epstein A, Shulman GL, & Corbetta M (2007). Breakdown of functional connectivity in frontoparietal networks Underlies behavioral deficits in spatial neglect. Neuron, 53(6), 905–918. 10.1016/j.neuron.2007.02.013. [PubMed: 17359924]

Latora V, & Marchiori M (2001). Efficient behavior of small-world networks. Physical Review Letters, 87(19), 198701 10.1103/PhysRevLett.87.198701. [PubMed: 11690461]

Laumann TO, Gordon EM, Adeyemo B, Snyder AZ, Joo SJ, Chen M-Y, et al. (2015). Functional system and areal organization of a highly sampled individual human brain. Neuron, 87(3), 657– 670. 10.1016/j.neuron.2015.06.037. [PubMed: 26212711]

Lazar RM, & Antoniello D (2008). Variability in recovery from aphasia. Current Neurology and Neuroscience Reports, 8(6), 497–502. [PubMed: 18957187]

Liepert J, Bauder H, Miltner WHR, Taub E, & Weiller C (2000). Treatment-induced cortical reorganization after stroke in humans. Stroke, 31(6), 1210–1216. 10.1161/01.STR.31.6.1210. [PubMed: 10835434]

Lim DH, LeDue JM, Mohajerani MH, & Murphy TH (2014). Optogenetic mapping after stroke reveals network-wide scaling of functional connections and heterogeneous recovery of the peri-infarct. The Journal of Neuroscience, 34(49), 16455–16466. 10.1523/JNEUROSCI.3384-14.2014. [PubMed: 25471583]

Lv Y, Margulies DS, Cameron Craddock R, Long X, Winter B, Gierhake D, et al. (2013). Identifying the perfusion deficit in acute stroke with resting-state functional magnetic resonance imaging. Annals of Neurology, 73(1), 136–140. 10.1002/ana.23763. [PubMed: 23378326]

Marcus DS, Harms MP, Snyder AZ, Jenkinson M, Wilson JA, Glasser MF, et al. (2013). Human connectome project informatics: Quality control, database services, and data visualization. Neuroimage, 80, 202–219. 10.1016/j.neuroimage.2013.05.077. [PubMed: 23707591]

Muldoon SF, Bridgeford EW, & Bassett DS (2016). Small-world propensity and weighted brain networks. Scientific Reports, 6(22057). 10.1038/srep22057.

Murphy TH, & Corbett D (2009). Plasticity during stroke recovery: From synapse to behaviour. Nature Reviews Neuroscience, 10(12), 861–872. 10.1038/nrn2735. [PubMed: 19888284]

Newman MEJ (2004). Fast algorithm for detecting community structure in networks. Physical Review E, 69(6), 066133 10.1103/PhysRevE.69.066133.

Nudo RJ, & Milliken GW (1996). Reorganization of movement representations in primary motor cortex following focal ischemic infarcts in adult squirrel monkeys. Journal of Neurophysiology, 75(5), 2144–2149. [PubMed: 8734610]

Onnela J-P, Saramaki J, Kertész J, & Kaski K (2005). Intensity and coherence of motifs in weighted complex networks. Physical Review E, 71(6), 065103 10.1103/PhysRevE.71.065103.

Petersen SE, & Sporns O (2015). Brain networks and cognitive architectures. Neuron, 88(1), 207–219. 10.1016/j.neuron.2015.09.027. [PubMed: 26447582]

Power JD, Barnes KA, Snyder AZ, Schlaggar BL, & Petersen SE (2012). Spurious but systematic correlations in functional connectivity MRI networks arise from subject motion. Neuroimage, 59(3), 2142–2154. 10.1016/j.neuroimage.2011.10.018. [PubMed: 22019881]

Power JD, Cohen AL, Nelson SM, Wig GS, Barnes KA, Church JA, et al. (2011). Functional network organization of the human brain. Neuron, 72(4), 665–678. 10.1016/j.neuron.2011.09.006. [PubMed: 22099467]

Power JD, Mitra A, Laumann TO, Snyder AZ, Schlaggar BL, & Petersen SE (2014). Methods to detect, characterize, and remove motion artifact in resting state fMRI. Neuroimage, 84, 320–341. 10.1016/j.neuroimage.2013.08.048. [PubMed: 23994314]

Power JD, Schlaggar BL, Lessov-Schlaggar CN, & Petersen SE (2013). Evidence for hubs in human functional brain networks. Neuron, 79(4), 798–813. 10.1016/j.neuron.2013.07.035. [PubMed: 23972601]

Prabhakaran S, Zarahn E, Riley C, Speizer A, Chong JY, Lazar RM, et al. (2007). Inter-individual variability in the capacity for motor recovery after ischemic stroke. Neurorehabilitation and Neural Repair. 10.1177/1545968307305302.

Ramsey LE, Siegel JS, Baldassarre A, Metcalf NV, Zinn K, Shulman GL, et al. (2016). Normalization of network connectivity in hemispatial neglect recovery. Annals of Neurology, 80(1), 127–141. 10.1002/ana.24690. [PubMed: 27277836]

Ramsey LE, Siegel JS, Lang CE, Strube M, Shulman GL, & Corbetta M (2017). Behavioural clusters and predictors of performance during recovery from stroke. Nature Human Behaviour, 1, 0038 10.1038/s41562-016-0038.

Robb RA, & Hanson DP (1991). A software system for interactive and quantitative visualization of multidimensional biomedical images. Australasian Physical & Engineering Sciences in Medicine, 14, 9–30. [PubMed: 2029243]

Rubinov M, & Sporns O (2010). Complex network measures of brain connectivity: Uses and interpretations. Neuroimage, 52(3), 1059–1069. 10.1016/j.neuroimage.2009.10.003. [PubMed: 19819337]

Satterthwaite TD, Wolf DH, Loughead J, Ruparel K, Elliott MA, Hakonarson H, et al. (2012). Impact of in-scanner head motion on multiple measures of functional connectivity: Relevance for studies of neurodevelopment in youth. Neuroimage, 60(1), 623–632. 10.1016/j.neuroimage.2011.12.063. [PubMed: 22233733]

Schmahmann JD, & Pandya DN (1997). The cerebrocerebellar system In Bradley RJ, Harris RA, Jenner P, & Schmahmann JD (Eds.), International review of neurobiology (Vol. 41, pp. 31–60). Academic Press 10.1016/S0074-7742(08)60346-3. [PubMed: 9378595]

Siegel JS, Mitra A, Laumann TO, Seitzman BA, Raichle M, Corbetta M, et al. (2016). Data quality influences observed links between functional connectivity and behavior. Cerebral Cortex. 10.1093/cercor/bhw253.

Siegel JS, Ramsey LE, Snyder AZ, Metcalf NV, Chacko RV, Weinberger K, et al. (2016). Disruptions of network connectivity predict impairment in multiple behavioral domains after stroke. Proceedings of the National Academy of Sciences of the United States of America, 113(30), E4367–E4376. 10.1073/pnas.1521083113. [PubMed: 27402738]

Siegel JS, Shulman GL, & Corbetta M (2017). Measuring functional connectivity in stroke: Approaches and considerations. Journal of Cerebral Blood Flow & Metabolism. 10.1177/0271678X17709198,0271678X1770919.

Siegel JS, Snyder AZ, Ramsey L, Shulman GL, & Corbetta M (2016). The effects of hemodynamic lag on functional connectivity and behavior after stroke. Journal of Cerebral Blood Flow & Metabolism, 36(12), 2162–2176. 10.1177/0271678X15614846. [PubMed: 26661223]

Smith SM, Fox PT, Miller KL, Glahn DC, Fox PM, Mackay CE, et al. (2009). Correspondence of the brain's functional architecture during activation and rest. Proceedings of the National Academy of Sciences of the United States of America, 106(31), 13040–13045. 10.1073/pnas.0905267106. [PubMed: 19620724]

Suzuki M, Sugimura Y, Yamada S, Omori Y, Miyamoto M, & Yamamoto J (2013). Predicting recovery of cognitive function soon after stroke: Differential modeling of logarithmic and linear regression. Plos One, 8(1), e53488 10.1371/journal.pone.0053488. [PubMed: 23326439]

Van Essen DC, Drury HA, Dickson J, Harwell J, Hanlon D, & Anderson CH (2001). An integrated software suite for surface-based analyses of cerebral cortex. Journal of the American Medical Informatics Association, 8(5), 443–459. 10.1136/jamia.2001.0080443. [PubMed: 11522765]

van Meer MP, Marel K. van der, Wang K, Otte WM, Bouazati S. el, Roeling TAP, et al. (2010). Recovery of sensorimotor function after experimental stroke correlates with restoration of resting-state interhemispheric functional connectivity. The Journal of Neuroscience, 30(11), 3964–3972. 10.1523/JNEUROSCI.5709-09.2010. [PubMed: 20237267]

Watson BD, Dietrich WD, Busto R, Wachtel MS, & Ginsberg MD (1985). Induction of reproducible brain infarction by photochemically initiated thrombosis. Annals of Neurology, 17(5), 497–504. 10.1002/ana.410170513. [PubMed: 4004172]

Watts DJ, & Strogatz SH (1998). Collective dynamics of 'small-world' networks. Nature, 393(6684), 440–442. 10.1038/30918. [PubMed: 9623998]

Wig GS (2017). Segregated systems of human brain networks. Trends in Cognitive Sciences, 21(12), 981–996. 10.1016/j.tics.2017.09.006. [PubMed: 29100737]

Winship IR, & Murphy TH (2009). Remapping the somatosensory cortex after stroke: Insight from imaging the synapse to network. The Neuroscientist, 15(5), 507–524. 10.1177/1073858409333076. [PubMed: 19622841]

Yeo BTT, Krienen FM, Sepulcre J, Sabuncu MR, Lashkari D, Hollinshead M, et al. (2011). The organization of the human cerebral cortex estimated by intrinsic functional connectivity. Journal of Neurophysiology, 106(3), 1125–1165. 10.1152/jn.00338.2011. [PubMed: 21653723]
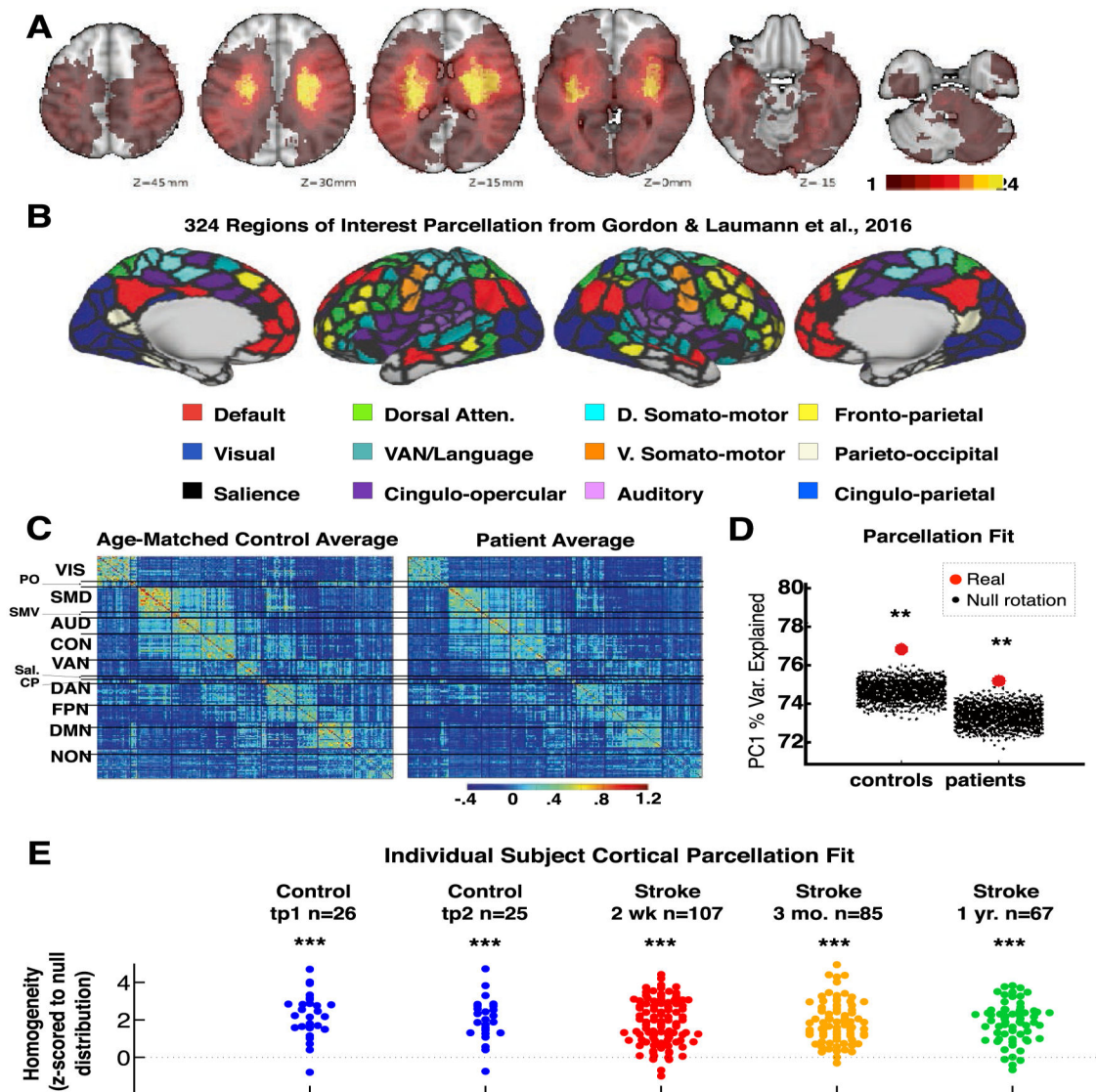
A

B

324 Regions of Interest Parcellation from Gordon & Laumann et al., 2016

■ Default	■ Dorsal Atten.	■ D. Somato-motor	■ Fronto-parietal
■ Visual	■ VAN/Language	■ V. Somato-motor	■ Parieto-occipital
■ Salience	■ Cingulo-opercular	■ Auditory	■ Cingulo-parietal

C Age-Matched Control Average   Patient Average

D Parcellation Fit

E Individual Subject Cortical Parcellation Fit

Fig. 1 –.

Functional brain areas defined in healthy young adults remain present across stages of stroke and recovery. A: Topography of stroke. Lesion overlay map in atlas space for 132 stroke patients. Lesion distribution is representative of a larger source population. B: 324 regions of interest parcellation from Gordon et al., 2016. Regions are color coded by RSN membership. C: Group-averaged parcel-wise functional connectivity. Average Fisher z-transformed FC matrices are shown for age-matched controls (n = 27) and stroke patients (n = 100) at timepoint 1. D: Homogeneity of group-averaged functional connectivity in acute stroke patients and age-matched controls compared to 1,000 null model iterations. In both groups the 324-region parcellation surpassed all 1,000 null models ($p < .001$). E: Parcellation homogeneity in individual subjects: patients (2 weeks, 3 months, 1 year) and controls (2 timepoints, 3 months apart). Difference between real homogeneity and 100 null model homogeneity is measured for each subject.
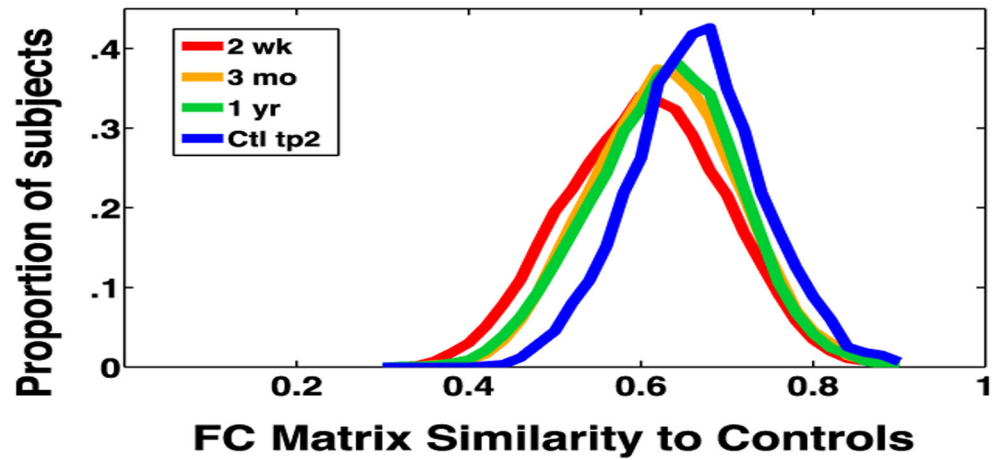
Fig. 2 –.
Group FC Similarity to controls. Pearson correlation between all members of a given group and control at timepoint 1. The X-axis is a simple measure of FC similarity. This measure is computed by turning the 324- by-324 FC matrix into a 52,326 vector for each subject. For a given group (i.e. patients at 2 weeks), a spatial correlation was computed between the FC vector of every subject and the FC vector of every subject in the control group. Each curve is a histogram of similarity values for one group. Similarity to controls increases between 2 weeks and 1year post-stroke (paired t-test: t = 3.9, $p < .0001$).
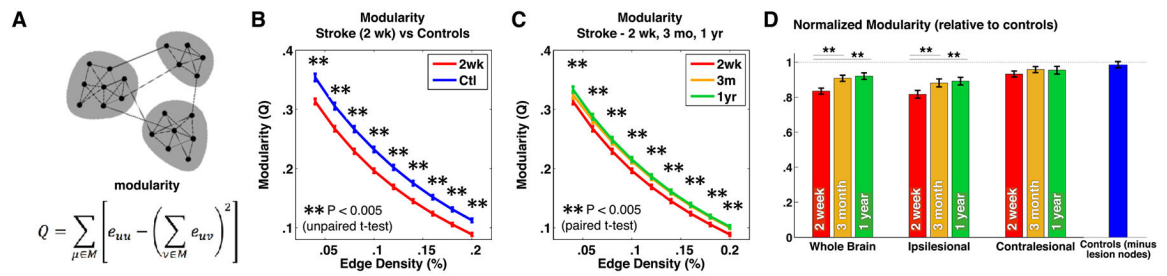
Fig. 3 –.

Behavior recovery following stroke is predicted by recovery of brain network modularity. A: Modularity measures the density of links inside communities compared to links between communities. Modularity is decreased in acute stroke patients (B), but returns to near control levels at 3 month and 1 year timepoints (C). D: Modularity, normalized to controls and averaged across densities (2–20%) is shown for the whole brain, ipsi-lesional, and contra-lesional hemisphere (compared to single hemisphere modularity in controls). ** indicates *p* < .005 (uncorrected) for an unpaired t-test between patients and controls in B and for a paired t-test between 2 weeks and 1 year for patients in C/D.
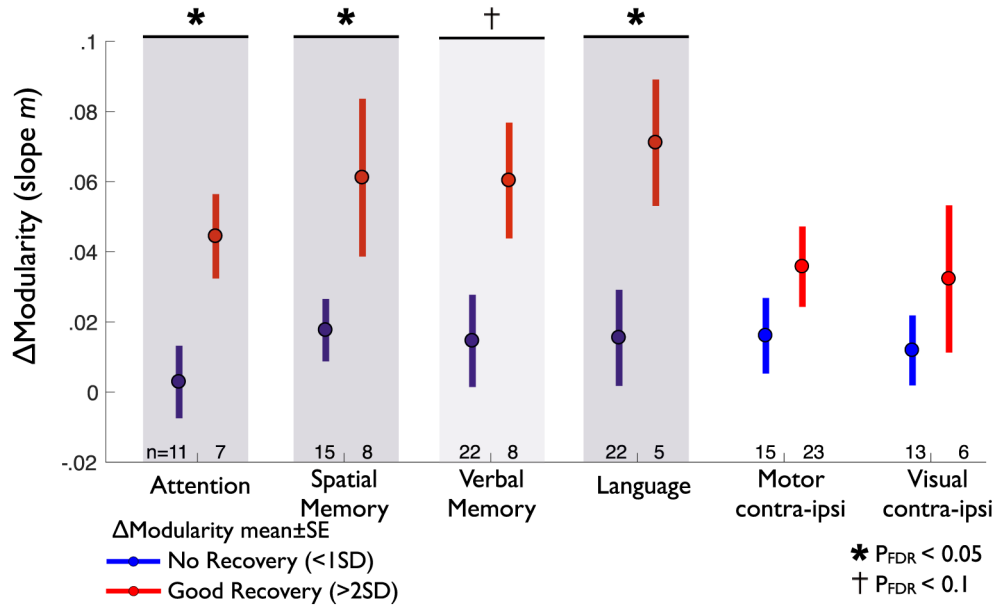
Fig. 4 –.

Recovery of modularity correlates with behavioral recovery. In each of six behavioral domains, modularity change is compared between poor recovery patients (Δbehavioral between 2 weeks and 1 year < 1SD), and good recovery patients (Δbehavioral > 2SD). Modularity change is measured as the slope m of the log model solved for modularity at 2 weeks, 3 months, and 1 year (Fig. S1). For each group, mean Δmodularity is indicated by a circle, with bars indicating standard error, the number of patients in each group is given below. In attention, language, and spatial memory, good behavioral recovery (red) show significantly greater increase in modularity than poor behavioral recovery (blue) (one-tailed unpaired t-test, $p < .05$ after correction for multiple comparisons). Verbal memory is trending towards significance ($p < .1$). ΔModularity is not significantly different between good versus poor recovery in motor and visual domains.
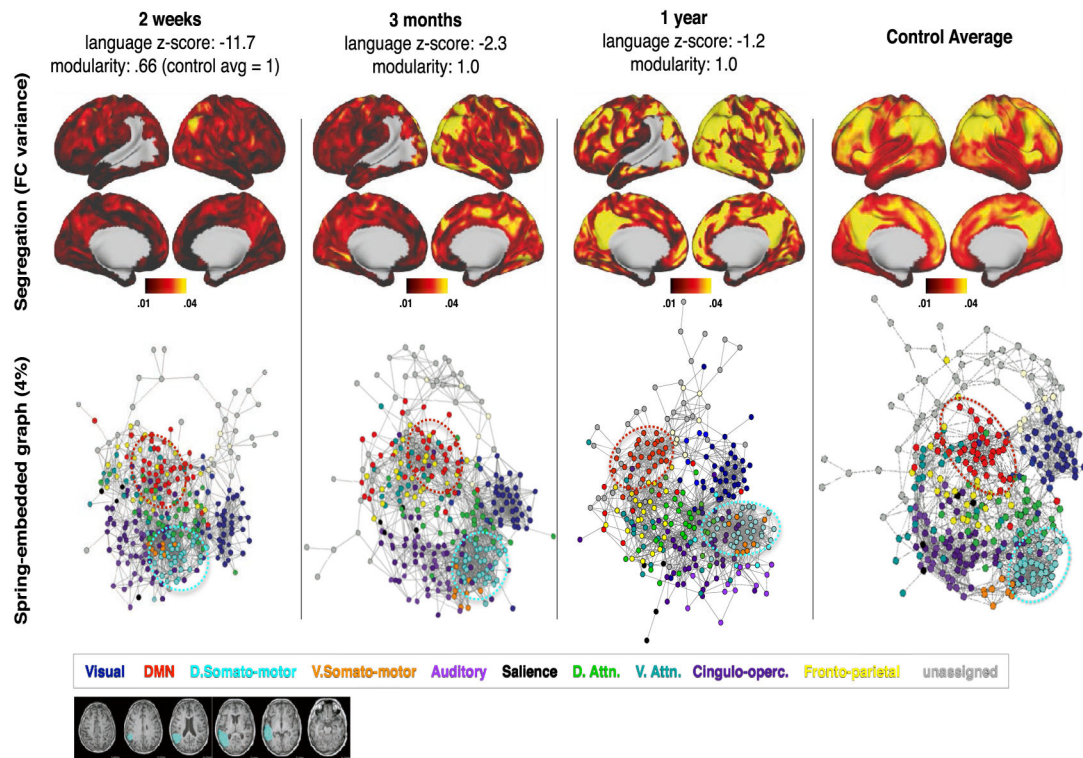
Fig. 5 –.

P108: Severe aphasia with good recovery paralleled by modularity recovery. At two weeks post-stroke, language performance was 11.7 standard deviations below age-matched controls. This improved to 2.3 at three months and 1.2 at one year. Network visualizations are given at all three timepoints, with control averages shown in the right-most column for reference. Top: vertex-wise segregation (FC variance), measured by variance in FC between a given surface vertex and all other brain areas greater than 20 mm away. Bottom: Spring-embedded network representation at 4% edge density, colored based on predefined communities (communities shown in Fig. 1B). Below: T1 MRI with lesion mask overlaid.
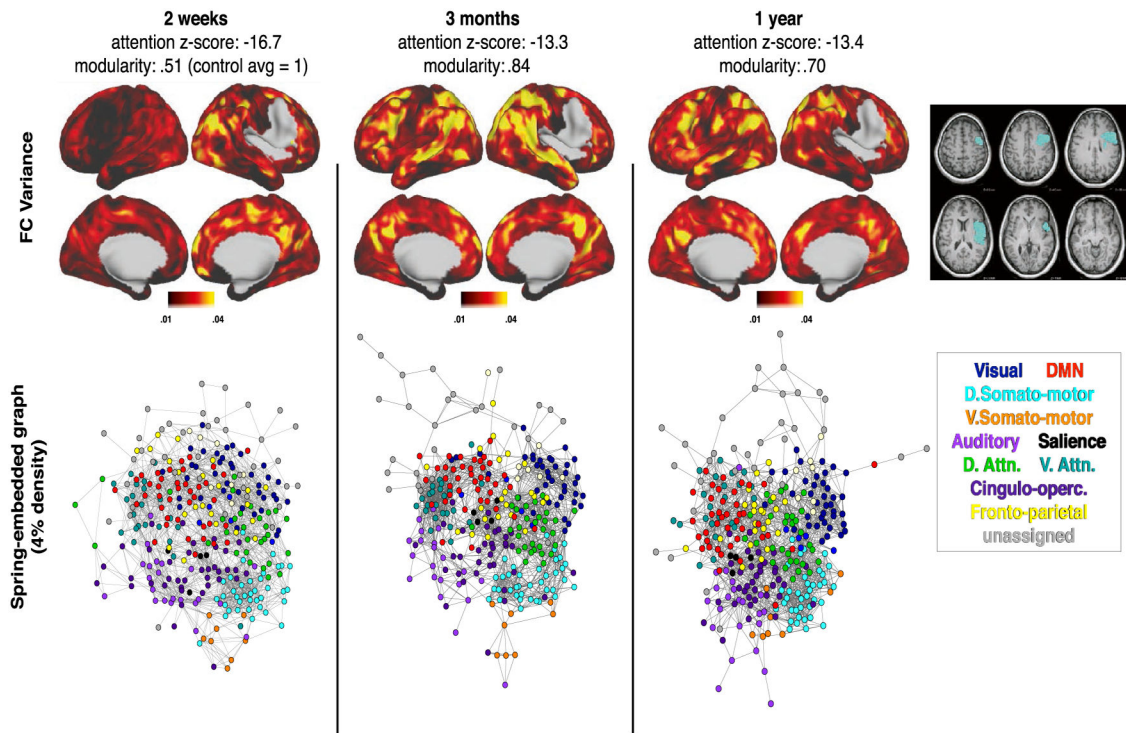
Fig. 6 –.

P30: Severe left hemi-neglect with poor recovery, low modularity throughout. Results are generated and displayed as in Fig. 5.
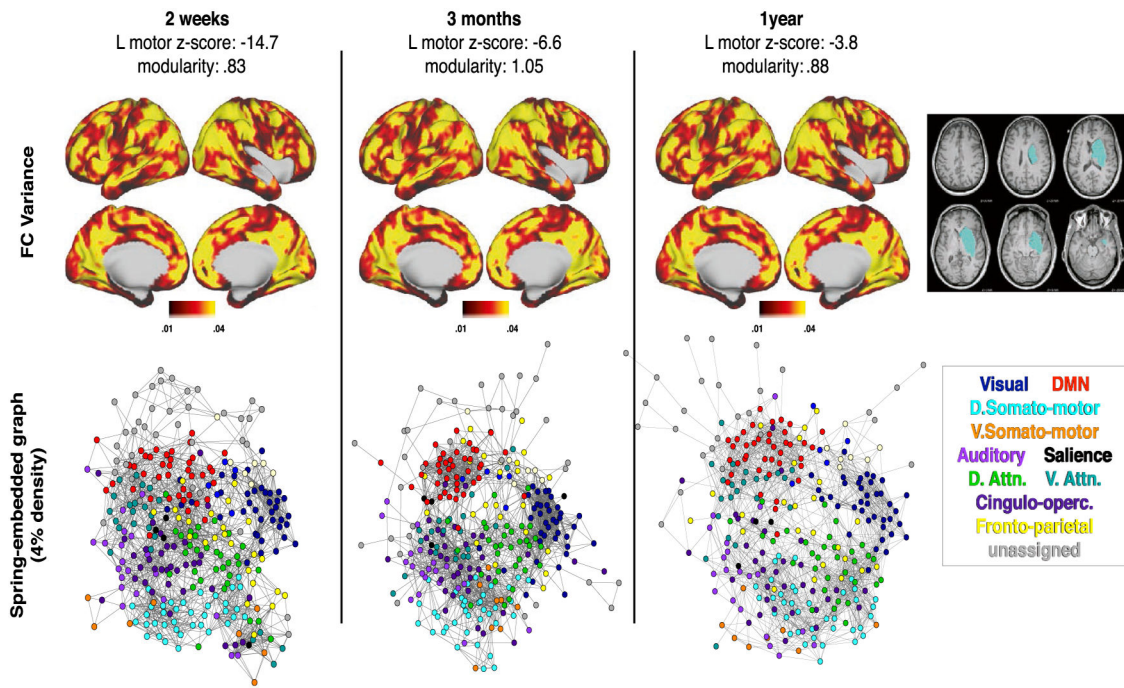
Fig. 7 –.

P161: Severe left hemiparesis with good recovery, minimal change in modularity by 1 year. Results are generated and displayed as in Fig. 5.
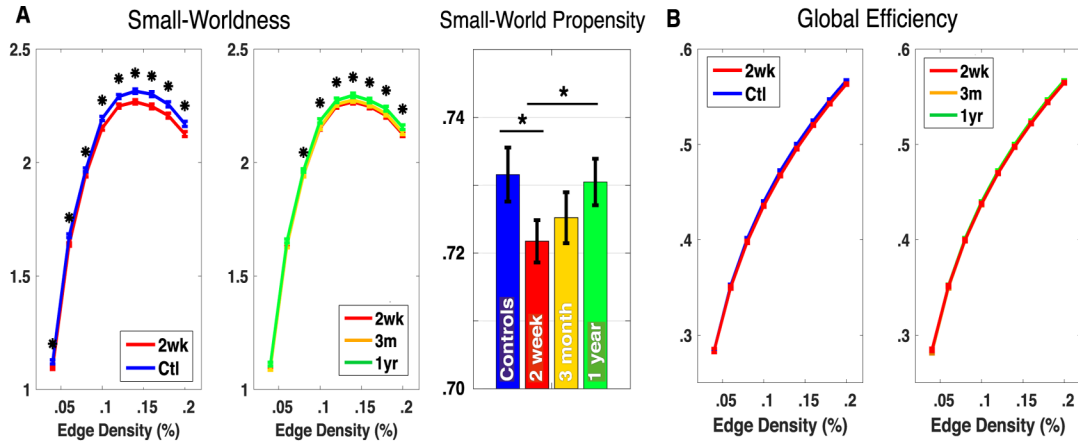
Fig. 8 –.
Small-Worldness, Small-World Propensity and Global Efficiency. A: Small-worldness (Eq. (4)) is compared over a range of edge densities between patients and controls (left) and over recovery (middle), and using small-world propensity on weighted networks (right). B: Global efficiency (Eq. (3)) is compared over a range of edge densities between patients and controls (left) and over recovery (right). * indicates $p < .05$ (uncorrected) for an unpaired t-test between patients and controls in for a paired t-test between 2 weeks and 1 year for patients. T-tests are not corrected for multiple comparisons because the measures are not independent.

Table 1

– Sample sizes and imaging quality metrics for controls, patients, and case study P108.

Table 1A		Timepoint 1	Timepoint 2
Controls	N	30	30
	N (incl.)	26	25
	Frames	571.4(210.0)	525.4(216.6)
	FD	.234(.062)	.246(.053)
	Lag	.191(.046)	.239(.136)

Table 1B		2 weeks	3 months	1 year
Patients	N	132	103	88
	N (incl.)	107	85	67
	Frames	596.0(209.6)	649.4(177.8)	632.9(177.8)
	FD	.231(.063)	.224(.057)	.223(.057)
	Lag	.182(.156)	.291(.156)	.276(.119)
P 108	Frames	737/896	644/896	637/896
	FD	.2392	.2495	.2408
	Lag	.1428	.1448	.1514